

# The softening phenomenon due to the curvature effect: in the case of extremely short intrinsic emission

Y.-P. Qin<sup>1,2</sup>

## ABSTRACT

Both the light curve and spectral evolution of the radiation from a relativistic fireball with extremely short duration are studied, in order to examine the curvature effect for different forms of the radiation spectrum. Assuming a  $\delta$  function emission we get formulas that get rid of the impacts from the intrinsic emission duration, applicable to any forms of spectrum. It shows that the same form of spectrum could be observed at different times, with the peak energy of the spectrum shifting from higher energy bands to lower bands following  $E_{peak} \propto t^{-1}$ . When the emission is early enough the  $t^2 f_\nu(t)$  form as a function of time will possess exactly the same form that the intrinsic spectrum as a function of frequency has. Assuming  $f_\nu \propto \nu^{-\beta} t^{-\alpha}$  one finds  $\alpha = 2 + \beta$  which holds for any intrinsic spectral forms. This relation will be broken down and  $\alpha > 2 + \beta$  or  $\alpha \gg 2 + \beta$  will hold at much later time when the angle between the moving direction of the emission area and the line of sight is large. An intrinsic spectrum in the form of the Band function is employed to display the light curve and spectral evolution. Caused by the shifting of the Band function spectrum, a temporal steep decay phase and a spectral softening appear simultaneously. The softening phenomenon will appear at different frequencies. It occurs earlier for higher frequencies and later for lower frequencies. The terminating softening time  $t_{s,max}$  depends on the observation frequency, following  $t_{s,max} \propto \nu^{-1}$ . This model predicts that the softening duration would be linearly correlated with  $t_{s,max}$ ; the observed  $\beta_{min}$  and  $\beta_{max}$  are determined by the low and high energy indexes of the Band function; both  $\beta_{min}$  and  $\beta_{max}$  are independent of the observation frequency.

*Subject headings:* gamma-rays: bursts — gamma-rays: theory — relativity

---

<sup>1</sup>Center for Astrophysics, Guangzhou University, Guangzhou 510006, P. R. China; ypqin@gzhu.edu.cn

<sup>2</sup>Physics Department, Guangxi University, Nanning 530004, P. R. China

## 1. Introduction

The successful launch of the Swift satellite (Gehrels et al. 2004) has made great advance for the observations of the X-ray afterglows of gamma-ray bursts (GRBs) in the past few years (for a recent review, see Zhang 2007). Among the many new findings obtained by the Swift instruments, some emerge as a puzzling. One is the spectral evolution which was detected in the tails of some bursts (Campana et al. 2006; Ghisellini et al. 2006; Gehrels et al. 2006; Mangano et al. 2007; Zhang et al. 2007a). The phenomenon has not been predicted by the curvature effect nor by the standard external shock afterglow model. Soon after that, Zhang et al. (2007b) performed a systematic analysis on this issue and found that 33 of the 44 bursts with bright steep decay tails show an obvious spectral evolution — an observed softening. This suggests that, the detected spectral evolution is not a rare phenomenon, but instead, it is quite common (at least detectable in the majority of GRBs that have bright steep decay tails).

Several attempts have been made to interpret this softening phenomenon. It was proposed that a central engine producing a soft but decaying afterglow emission might be responsible for some of these bursts (Campana et al. 2006; Fan et al. 2006; Zhang et al. 2007b). Some bursts with strong softening might be accounted for by a cooling of the internal-shocked region (Zhang et al. 2007b). A possible thermal component has also been tried. However, Yonetoku et al. (2008) showed that introducing a thermal component is not sufficient to explain all of the spectral softening, and thus additional spectral evolution is required. In investigating the origins for the spectral evolution of GRB 070616, Starling et al. (2008) ruled out the possibility that a superposition of two power-laws causes the evolution. In stead, they considered a possibility of an additional component dominant during the late prompt emission. They proposed that a combination of the spectral evolution and the curvature effect may cause the observed steep decay phase of the light curve. Another scenario is based on the cannonball model of GRBs, which was suggested to be responsible for both the temporal behavior and the spectral softening of the bursts observed by Swift (Dado et al. 2008).

As shown in Zhang et al. (2007b), the spectral softening is accompanied by a very steep decay phase. This phase is seen directly following the prompt emission and is naturally (and generally) regarded as the tail of the prompt emission (Tagliaferri et al. 2005; Barthelmy et al. 2005; Liang et al. 2006). The tail was suspected to arise from the emission of the high latitude of the fireball surface, which is often referred to as the curvature effect (Kumar & Panaitescu 2000; Dermer 2004; Dyks et al. 2005; Liang et al. 2006; Panaitescu et al. 2006; Zhang et al. 2006, 2007b; Butler & Kocevski 2007; Qin 2008; Starling et al. 2008). A full consideration of the curvature effect includes the delay of time and the shifting of

the intrinsic spectrum as well as other relevant factors of an expanding fireball (for detailed explanation and analysis, see Qin 2002; Qin et al. 2004, 2006; Qin 2008). The effect has been intensively studied in the prompt gamma-ray phase, such as the profile of the light curve of pulses, the spectral lags, the power-law relation between the pulse width and energy, the evolution of the hardness ratio and the evolution of the peak energy (Fenimore et al. 1996; Sari & Piran 1997; Qin 2002; Ryde & Petrosian 2002; Kocevski et al. 2003; Qin & Lu 2005; Shen et al. 2005; Lu et al. 2006, 2007; Peng et al. 2006; Qin et al. 2004, 2005, 2006; Jia 2008).

In a recent investigation, Butler & Kocevski (2007) concluded that the early emission in  $> 90\%$  of early afterglows has a characteristic  $\nu f_\nu$  spectral energy  $E_{peak}$ , which likely evolves from the  $\gamma$ -rays through the soft X-ray band on timescales of  $10^2 - 10^4$  s after the GRB. Many careful analyses revealed that there do exist some bursts with their peak energy  $E_{peak}$  decreasing from a higher band to a much lower band. These bursts include: GRB 060124, from 108 keV to 1.3 keV (Butler & Kocevski 2007); GRB 060614, from 8.6 keV to 1.1 keV (Butler & Kocevski 2007; Mangano et al. 2007); GRB 060904A, from 163 keV to 2.28 keV (Yonetoku et al. 2008); GRB 061121, from 270 keV to 0.95 keV (Butler & Kocevski 2007); GRB 070616, from 135 keV to  $\sim 4$  keV (Starling et al. 2008). For GRB 070616, the spectral softening evolution was observed even in the prompt emission phase: its duration is  $T_{90} = 402.4s$ , while the softening starts from 285s and extends to 1200s (Starling et al. 2008). Among them, GRB 060614, GRB 060904A and GRB 061121 are members of the Zhang et al. (2007b)'s sample. Although the curvature effect was rejected to interpret the softening by some authors, Starling et al. (2008) insisted that the observed shifting of the peak energy is in agreement with what expected by the curvature effect: the peak energy of the Band function spectrum passes through the  $\gamma$ -ray band at a relatively early time, while it passes through the X-ray band at a later time due to the high latitude emission. They proposed that both the curvature effect and a strong spectral evolution cause the steep decline in flux. Based on the explicit illustration of the evolution of the whole spectral form in Butler & Kocevski (2007), we suspect that the curvature effect alone might be responsible for both the spectral softening and the accompanied step decay light curve.

To reveal the pure curvature effect and get rid of the possible impacts from the emission duration, we concern in this paper only extremely short intrinsic emission. Focusing on this emission has two advantages. The first is that the formulas become very simple, and the second is that many key characteristics of the effect can be plainly illustrated. The paper is organized as follows. In Section 2, we present basic formulas of the full curvature effect, applicable to any temporal and spectral forms of emission. We discuss light curves and spectral evolution arising from an extremely short emission in Section 3. In Section 4, we assume an intrinsic spectrum in the form of the Band function and illustrate the

corresponding light curve and spectral evolution in detail. Parameters that affect the results are discussed in Section 5. In Section 6, we apply the model to the XRT band and also to a Swift burst. Discussion and conclusions are presented in Section 7.

## 2. Equations of flux densities influenced by the curvature effect

In the following, we study the emission from an expanding fireball shell. Suppose the emission occurs over the fireball area confined by  $\theta_{\min} \leq \theta \leq \theta_{\max}$ , where  $\theta$  is the angle between the normal of the area concerned with respect to the line of sight (which is also the angle of the moving direction of the emitting region with respect to the direction to the observer), and within proper time interval  $t_{0,\min} \leq t_0 \leq t_{0,\max}$ . Let us consider the following situation: the Lorentz factor of the emitting shell is constant, the energy range of the emission is unlimited, and the intrinsic radiation intensity is independent of direction. Basic formulas of the flux density which is expected by a distant observer measured at laboratory time  $t_{ob}$  and other relevant quantities for this simple situation are presented in Qin (2008; see equations 1-5 there).

To meet and/or approximate the conventional definition of observation time, we assign (see also Qin 2008)

$$t \equiv t_{ob} - t_c + R_c/v - D/c, \quad (1)$$

where  $t_c$  as a time constant is defined in the observer frame,  $D$  is the distance of the fireball to the observer,  $v$  is the speed of the shell,  $R_c$  is the radius of the shell measured at  $t_c$  by local observers who are stationary in the explosion area. Equation (1) is a definition of observation time. With this definition of time, the basic formulas can be written as

$$f_\nu(t) = \frac{2\pi c^2}{D^2(\Gamma v/c)^2 t^2} \int_{\tilde{t}_{0,\min}}^{\tilde{t}_{0,\max}} I_{0,\nu}(t_0, \nu_0) [R_c/c + (t_0 - t_{0,c})\Gamma v/c]^2 [(t_0 - t_{0,c})\Gamma + R_c/v - t] dt_0, \quad (2)$$

with

$$\tilde{t}_{0,\min} = \max\left\{t_{0,\min}, \frac{t - R_c/v + (R_c/c) \cos \theta_{\max}}{[1 - (v/c) \cos \theta_{\max}]\Gamma} + t_{0,c}\right\}, \quad (3)$$

$$\tilde{t}_{0,\max} = \min\left\{t_{0,\max}, \frac{t - R_c/v + (R_c/c) \cos \theta_{\min}}{[1 - (v/c) \cos \theta_{\min}]\Gamma} + t_{0,c}\right\}, \quad (4)$$

$$\nu_0 = \frac{t}{R_c/v + (t_0 - t_{0,c})\Gamma} \Gamma \nu, \quad (5)$$

and

$$\begin{aligned} & [1 - (v/c) \cos \theta_{\min}] [(t_{0,\min} - t_{0,c})\Gamma + R_c/v] \leq t \\ & \leq [1 - (v/c) \cos \theta_{\max}] [(t_{0,\max} - t_{0,c})\Gamma + R_c/v] \end{aligned} \quad (6)$$

where  $t_{0,c}$  denotes the moment of  $t_c$ , measured by a co-moving observer;  $I_{0,\nu}(t_0, \nu_0)$  is the intrinsic radiation intensity;  $\Gamma = 1/\sqrt{1 - v^2/c^2}$ . Equations (2)-(6) are more general than equations (8)-(12) in Qin (2008). The former can be applied to any forms of the intrinsic spectrum, while the later are applicable only in the case of a single power-law spectrum. According to equation (1), referring also to equation (8) in Qin et al. (2004),  $t = 0$  corresponds to the moment of the emission that occurs at the spot of the explosion (say,  $R_c = 0$ ). Or precisely,  $t = 0$  is the moment when photons emitted from  $R_c = 0$  reach the observer. As explained in Qin (2008), observation time  $t$  approximates the time defined by the trigger time (e.g.,  $t = t_{ob} - t_{ob,trig}$ ). As long as the Lorentz factor is large enough and the trigger event is early enough, the offset between the two definitions of observation time would be very small (Qin 2008).

### 3. Light curves and the spectral evolution of the fireball arising from an extremely short intrinsic emission

The simplest emission is a  $\delta$  function emission which can always simplify the equations concerned. Perhaps the most important reason for considering a  $\delta$  function emission is that effects arising from the duration of real intrinsic emission will be omitted and therefore those merely coming from the expanding motion of the fireball surface will be clearly seen (Qin 2008). In practical situation, when an emission is extremely short, one could regard it as a  $\delta$  function emission. In order to reveal the main properties of the curvature effect in the case of X-ray afterglow, we consider only this kind of radiation and hence assume a  $\delta$  function emission through out this paper.

Let the concerned intrinsic emission be

$$I_{0,\nu}(t_0, \nu_0) = I_{0,0} \delta\left(\frac{t_0}{t_{0,0}} - \frac{t_{0,c}}{t_{0,0}}\right) g_\nu(\nu_0), \quad (7)$$

where  $t_{0,0} > 0$  is any assigned time constant (e.g.,  $t_{0,0} = 1s$ ),  $I_{0,0}$  is a constant in units of  $erg \cdot cm^{-2} s^{-1} Hz^{-1}$ , and  $g_\nu(\nu_0)$  is the intrinsic spectrum of the emission in a dimensionless form. We consider the emission from the whole fireball surface and take  $\theta_{\min} = 0$  and  $\theta_{\max} = \pi/2$ . In this situation, one gets from (6) that (see also Qin 2008)

$$(1 - v/c)R_c/v \leq t \leq R_c/v. \quad (8)$$

Within this observation time interval, equation (2) becomes

$$f_\nu(t) = \frac{2\pi I_{0,0} t_{0,0} R_c^2}{D^2 (\Gamma v/c)^2} \frac{g_\nu[\nu_0(t_0 = t_{0,c})] (R_c/v - t)}{t^2}. \quad (9)$$

According to equation (5),  $\nu_0$  is related to  $t$  and  $\nu$  by

$$\nu_0 = \frac{\Gamma v}{R_c} t \nu. \quad (10)$$

Inserting equation (10) into equation (9) comes to a plain result:

$$f_\nu(t) = \frac{2\pi I_{0,0} t_{0,0} R_c^2}{D^2 (\Gamma v/c)^2} (R_c/v - t) g_\nu \left( \frac{\Gamma v}{R_c} t \nu \right) t^{-2}. \quad (11)$$

A straightforward consequence of equation (11) comes from the situation when  $g_\nu(\nu_0) \propto \nu_0^{-\beta}$ , that gives rise to  $f_\nu(t) \propto (R_c/v - t) t^{-2-\beta} \nu^{-\beta}$  (see Qin 2008). When the event occurs early enough, the  $R_c/v - t$  term will become constant and then we come to the well-known form of flux density  $f_\nu(t) \propto t^{-2-\beta} \nu^{-\beta}$  (Fenimore et al. 1996; Kumar & Panaitescu 2000; Qin 2008).

Several conclusions are reached from equation (11). a) For a certain observation time satisfying equation (8), the spectrum observed is merely a shifted intrinsic one. The shifting factor is  $\Gamma v t / R_c$ . The peak energy will decline following  $E_{peak} = E_{peak,0} R_c / \Gamma v t$  (namely,  $E_{peak} \propto t^{-1}$ ). b) For a certain observation frequency, the light curve observed depends entirely on the emission spectrum. In the case when  $R_c/v \gg t$ , the form  $t^2 f_\nu(t)$ ,  $\propto g_\nu(\frac{\Gamma v t}{R_c})$ , as a function of time takes the same form that the intrinsic spectrum as a function of frequency has. Or, from  $t^2 f_\nu(t)|_{\nu=const}$ , when replacing  $t$  with variable  $\nu$  and multiplying it with a constant to alter its dimension one will get exactly the intrinsic spectral form (this might be useful in checking the curvature effect in further investigations). This is plain in the pure power-law emission where  $f_\nu(t) \propto t^{-2-\beta} \nu^{-\beta}$  in the case  $R_c/v \gg t$ . But the conclusion holds for any intrinsic spectral forms, which is unaware previously. As explained in Qin (2008), the term  $R_c/v - t$  reflects the projected factor of the infinitesimal fireball surface area in the angle concerned to the distant observer, known as  $\cos \theta$  (in fact,  $R_c/v - t$  is  $\cos \theta$  multiplying a constant; see Appendix A). When the emission area is close to the line of sight region, condition  $R_c/v \gg t$  (i.e.,  $\cos \theta \sim 1$ ) can easily be satisfied, while when the angle between the moving direction of the emission region and the line of sight is large enough the term  $R_c/v - t$  will be important. At a much later time, the emission area would be close to that of  $\theta = \pi/2$ , and the term  $R_c/v - t$  and then the flux will approach to zero (see Appendix A and Appendix B). c) Under the condition of  $R_c/v \gg t$ , which will hold at an earlier time, the temporal power law index and the spectral power law index will be well related. For a given time  $t$  and a given frequency  $\nu$ , we assign the flux as  $f_\nu(t) = f_0 t^{-\alpha}$  and assign the intrinsic spectrum as  $g_\nu(\frac{\Gamma v}{R_c} t \nu) = g_0 \cdot (\frac{\Gamma v}{R_c} t \nu)^{-\beta}$ . These can easily be satisfied when one carefully chooses  $f_0$ ,  $\alpha$ ,  $g_0$  and  $\beta$  in the vicinity of  $t$  (e.g., by performing a fit). Inserting  $g_\nu(\frac{\Gamma v}{R_c} t \nu) = g_0 \cdot (\frac{\Gamma v}{R_c} t \nu)^{-\beta}$  into  $f_\nu(t) = f_0 t^{-\alpha}$  under the  $R_c/v \gg t$  condition one will come to

the well-known  $\alpha = 2 + \beta$  relation from equation (11). Note that this relation will hold for any intrinsic spectral forms as long as the condition  $R_c/v \gg t$  is satisfied. When the angle  $\theta$  is large enough (say, when  $R_c/v - t \ll R_c/c$ ; see Appendix A) the  $\alpha = 2 + \beta$  relation will be broken down since the influence of the  $R_c/v - t$  term on the differential of the light curve (which is associated with  $\alpha$ ) will no more be ignored.

#### 4. In the case of the Band function spectrum

According to the above analysis, for an extremely short emission burst, its observed spectrum and its intrinsic spectrum take the same form. It is known that the observed spectra of most GRBs possess the Band function form (Band et al. 1993). Since emission from some of such bursts might be extremely short, it is likely that the intrinsic emission of some bursts takes the Band function form. In this section, we consider an intrinsic Band function emission and assume (Band et al. 1993)

$$g_\nu(\nu_0) = \begin{cases} \left(\frac{\nu_0}{\nu_{0,p}}\right)^{1+\alpha_{B,0}} \exp[-(2 + \alpha_{B,0})\frac{\nu_0}{\nu_{0,p}}] & \left(\frac{\nu_0}{\nu_{0,p}} < \frac{\alpha_{B,0}-\beta_{B,0}}{2+\alpha_{B,0}}\right) \\ \left(\frac{\alpha_{B,0}-\beta_{B,0}}{2+\alpha_{B,0}}\right)^{\alpha_{B,0}-\beta_{B,0}} \exp(\beta_{B,0} - \alpha_{B,0})\left(\frac{\nu_0}{\nu_{0,p}}\right)^{1+\beta_{B,0}} & \left(\frac{\alpha_{B,0}-\beta_{B,0}}{2+\alpha_{B,0}} \leq \frac{\nu_0}{\nu_{0,p}}\right) \end{cases}, \quad (12)$$

where  $\nu_{0,p}$ ,  $\alpha_{B,0}$ , and  $\beta_{B,0}$  are constants.

With this spectral form, we can produce the light curve and the spectral evolution using equation (11). In the following analysis we take  $\Gamma = 100$ ,  $R_c = 10^{15} \text{ cm}$ ,  $1 + \alpha_{B,0} = -0.5$ ,  $1 + \beta_{B,0} = -2.5$ , and  $h\nu_{0,p} = E_{0,p} = 1 \text{ keV}$  as a primary set of parameters. In the consequent analysis below they will be replaced one by one to reveal their influences on the light curve and the spectral evolution. We assign  $F_0 \equiv 2\pi I_{0,0} R_c^2 / D^2 (\Gamma v/c)^2$  and  $t_{0,0} = 1 \text{ s}$ . The flux density will be calculated in units of  $F_0$  through out this paper.

##### 4.1. Expected at the 1 keV observation frequency

First, let us explore the spectral evolution at  $E = 1 \text{ keV}$  by assuming a power law of flux within a limited (or narrow) band including  $E = 1 \text{ keV}$ :

$$f_\nu(t) = I(t)\nu^{-\beta}. \quad (13)$$

The resulting light curve and spectral evolution are displayed in Fig. 1. A temporal steep decay phase and a spectral softening are observed within the range of  $1 - 10^3 \text{ s}$ , which occur simultaneously. Determined or influenced by the intrinsic spectral form, the light curve

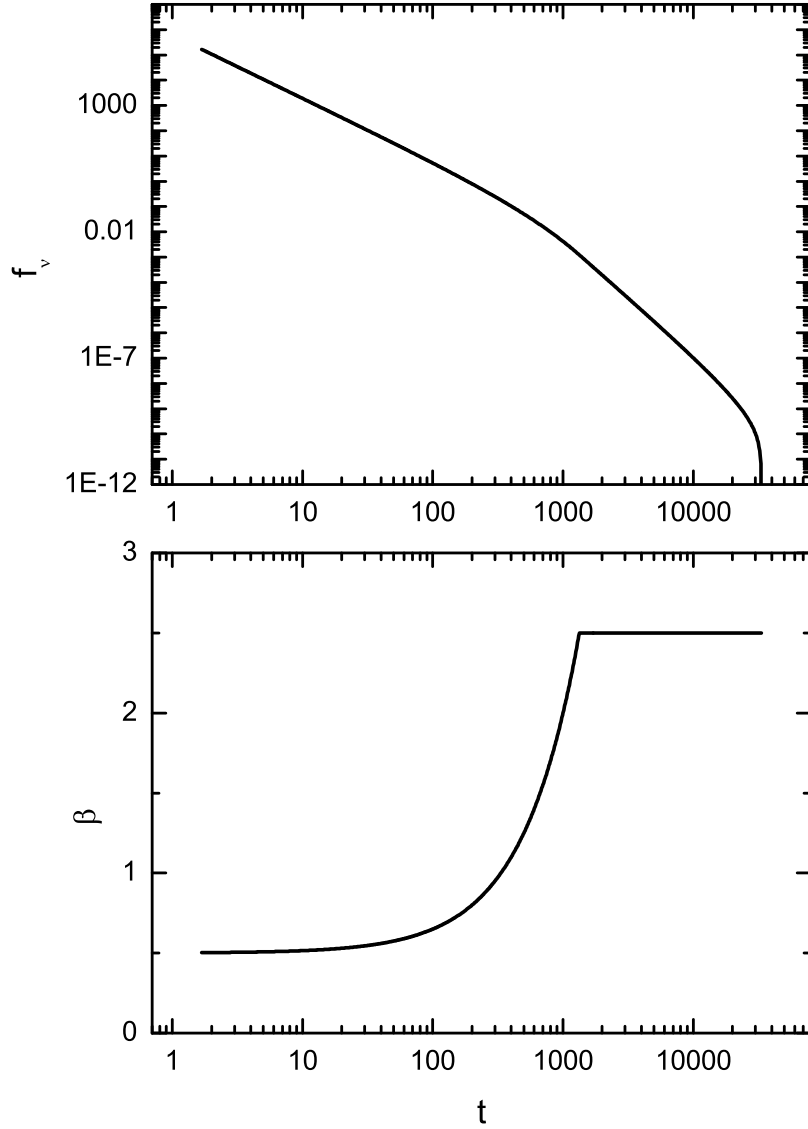


Fig. 1.— The light curve (the upper panel) and spectral evolution (the lower panel) of a  $\delta$  function emission from an expanding fireball, expected at 1 keV observation frequency. Observation time  $t$  is defined by equation (1) and in units of  $s$ . The flux density is calculated with equation (11) and in units of  $F_0$  [ $F_0 \equiv 2\pi I_{0,0} R_c^2 / D^2 (\Gamma v/c)^2$ ], while the intrinsic spectrum is determined by equation (12). The adopted parameters include:  $\Gamma = 100$ ,  $R_c = 10^{15} \text{ cm}$ ,  $1 + \alpha_{B,0} = -0.5$ ,  $1 + \beta_{B,0} = -2.5$ , and  $h\nu_{0,p} = 1 \text{ keV}$ . Equation (13) is used to defined and evaluate the spectral index  $\beta$ .

decays in a milder manner at an earlier time (influenced by the lower energy index of the Band function) and then turns to be steeper at a much later time (influenced by the higher energy index of the Band function). Connecting these two segments is a breaking feature which appears when the peak energy of the spectrum passes through the observation band (here, the 1 keV observation frequency). This feature is also viewable in Fig. 1 of Kumar & Panaitescu (2000) (at  $\sim 400$  s), and it is interpreted as due to the passing through the observation band as well. We observe that, at about 1400 s, the softening stops and the spectral index becomes constant. This occurs after the peak energy has sufficiently passing through the observation band. At about 30000 s, the light curve ends with a cutoff tail which is determined by the term  $R_c/v - t$ . As mentioned above, the term  $R_c/v - t$  comes from the projected factor of the infinitesimal fireball surface area in the angle concerned (say,  $\theta$ ) to the distant observer, known as  $\cos\theta$ . As the angle between the moving direction of the dominant emission area and the line of sight becomes larger, the  $\cos\theta$  term becomes smaller. When  $\theta$  approaches to  $\pi/2$  (the edge of the half fireball surface that faces the observer),  $\cos\theta$  approaches to zero and then the tail comes into being (it is expectable that any emission from a fireball must be limited due to its limited size).

The observed XRT light curves are ranging from 60s to  $1 \times 10^7$ s and from  $5 \times 10^{-15} \text{erg} \cdot \text{cm}^{-2} \text{s}^{-1}$  to  $8 \times 10^{-8} \text{erg} \cdot \text{cm}^{-2} \text{s}^{-1}$ . From the data of Fig. 1 we find that, at 60s  $f_\nu \sim 20F_0$ , at 1000s  $f_\nu \sim 4 \times 10^{-3}F_0$  (where the breaking feature appears), and at 30000s  $f_\nu \sim 1 \times 10^{-10}F_0$  (where the light curve cutoff tail, or the broken down feature, emerges). For the adopted parameter set, the flux at 1000s is smaller than that at 60s about 4 orders of magnitude, and then the breaking feature is reasonably expectable. The broken down feature cannot be observable since the flux associated with it is smaller than that at 60s about 11 orders of magnitude. However, this does not mean that this feature will never be observable since the magnitude of the flux associated with it depends strongly on the fireball radius, the intrinsic peak energy, and the energy indexes of the Band function spectrum. For example, for a much smaller high energy index [say, when  $-(1 + \beta_{B,0})$  is much smaller] the problem will be significantly eased, and for a smaller fireball radius the interval between the observable start time of the XRT light curve and the broken down feature will be much shorter and the difference between their flux magnitudes will be much smaller (see Fig. 6 and also the discussion below).

Development of the whole spectrum over the same period concerned is displayed in Fig. 2, where the  $\nu f_\nu$  curves at 5, 10, 50, 100, 500, 1000, 5000, and 10000 s, spanning from 0.01 to 1000 keV, are presented. This figure plainly illustrates that, due to the contribution of the high latitude emission (where angle  $\theta$  becomes larger and larger), it is indeed that the shifting of the Band function spectrum causes the softening observed in Fig. 1. When the peak energy has passed through the adopted bandpass (say, the 1 keV observation frequency), the higher

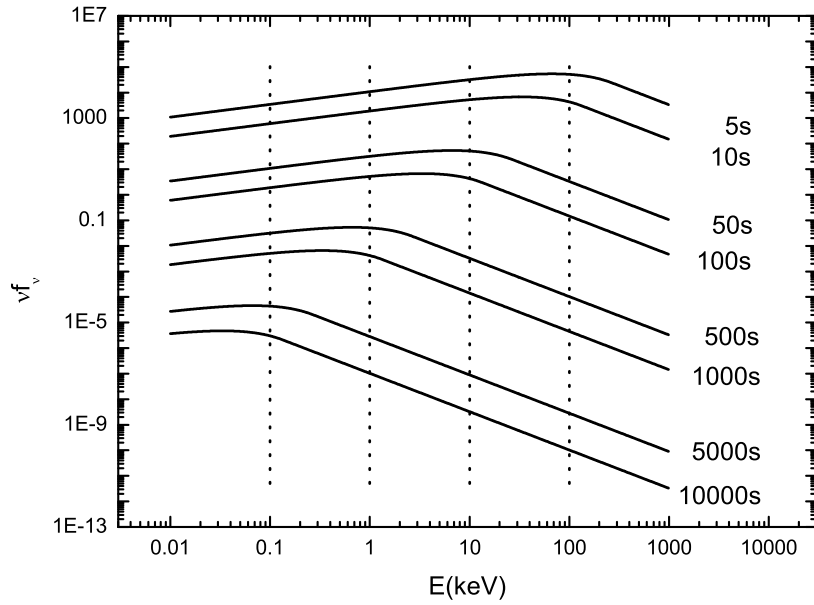


Fig. 2.— The  $\nu f_\nu$  (in units of  $F_0 \text{keV}$ ) spectra of the emission considered in Fig. 1, at different observation times. The four dotted lines represent the 0.1, 1, 10, and 100 keV frequencies respectively.

energy power law portion in the intrinsic Band function spectrum gradually dominates the emission. After  $\sim 1000$  s, the expected flux density (at  $h\nu = 1\text{keV}$ ) is mainly contributed by this emission (i.e., the  $\nu_0^{1+\beta_{B,0}}$  portion emission), and then the  $t^{-2-\beta}\nu^{-\beta}$  curve comes into being (here  $-\beta = 1 + \beta_{B,0}$ ). In this period, the spectral index  $\beta$  is of course constant (see Fig. 1). As mentioned above, the  $t^{-2-\beta}\nu^{-\beta}$  curve is deduced by assuming an intrinsic emission with a power law spectrum, emitted from an expanding fireball (Fenimore et al. 1996; Kumar & Panaitescu 2000; Qin 2008), which is a consequence of equation (11).

The evolution of the peak energy is shown in Fig. 3, where the  $E_{peak} \propto t^{-1}$  law is visible.

The  $\alpha = 2 + \beta$  relation discussed in last section can be directly checked by plotting and comparing the  $\alpha$  vs.  $t$  curve and the  $2 + \beta$  vs.  $t$  curve. This is shown in Fig. 4. When the observation time is not too late (say,  $< 2000$  s), the  $\alpha = 2 + \beta$  relation firmly stands. As expected, at later times the  $\alpha = 2 + \beta$  relation is broken down as the  $\cos\theta$  term (the  $R_c/v - t$  term) becomes important. This happens at  $\sim 2000$  s. After that, the  $\cos\theta$  term dominates the flux, and then the temporal index  $\alpha$  rapidly increases.

#### 4.2. Expected at other observation frequencies

Next, let us consider the light curve and spectral evolution expected at other observation frequencies. One finds from Fig. 2 that the peak energy passes through 0.1 keV frequency at a much later time while it passes through 100 keV at a very early time. This suggests that for the adopted set of parameters, the softening would appear at lower and very higher energy bands as well, but the corresponding times would be very different. Displayed in Fig. 5 are the light curves and the spectral evolution expected at frequencies 0.1, 1, 10 and 100 keV respectively. The spectral index  $\beta$  reaches its maximum at  $\sim 1.3 \times 10^4$ ,  $1.3 \times 10^3$ ,  $1.3 \times 10^2$  and 13 s, for frequencies 0.1, 1, 10 and 100 keV, respectively.

This analysis leads to the following conclusions: the softening due to the curvature effect will appear at different frequencies; it occurs earlier for higher frequencies and later for lower frequencies; the terminating softening time (defined as the time when the spectral index  $\beta$  reaches its maximum),  $t_{s,max}$ , depends strictly on the observation frequency, and it follows the  $t_{s,max} \propto \nu^{-1}$  law, where  $\nu$  is the observation frequency. Note that the  $t_{s,max} \propto \nu^{-1}$  law can also be deduced from equation (10) and/or equation (11). This prediction holds as long as the intrinsic emission is short enough.

Indeed, the spectral softening evolution was observed in the prompt emission of GRB 070616, starting from 285s and extending to 1200s (Starling et al. 2008). This favors our new finding that the softening is also expectable in higher energy bands.

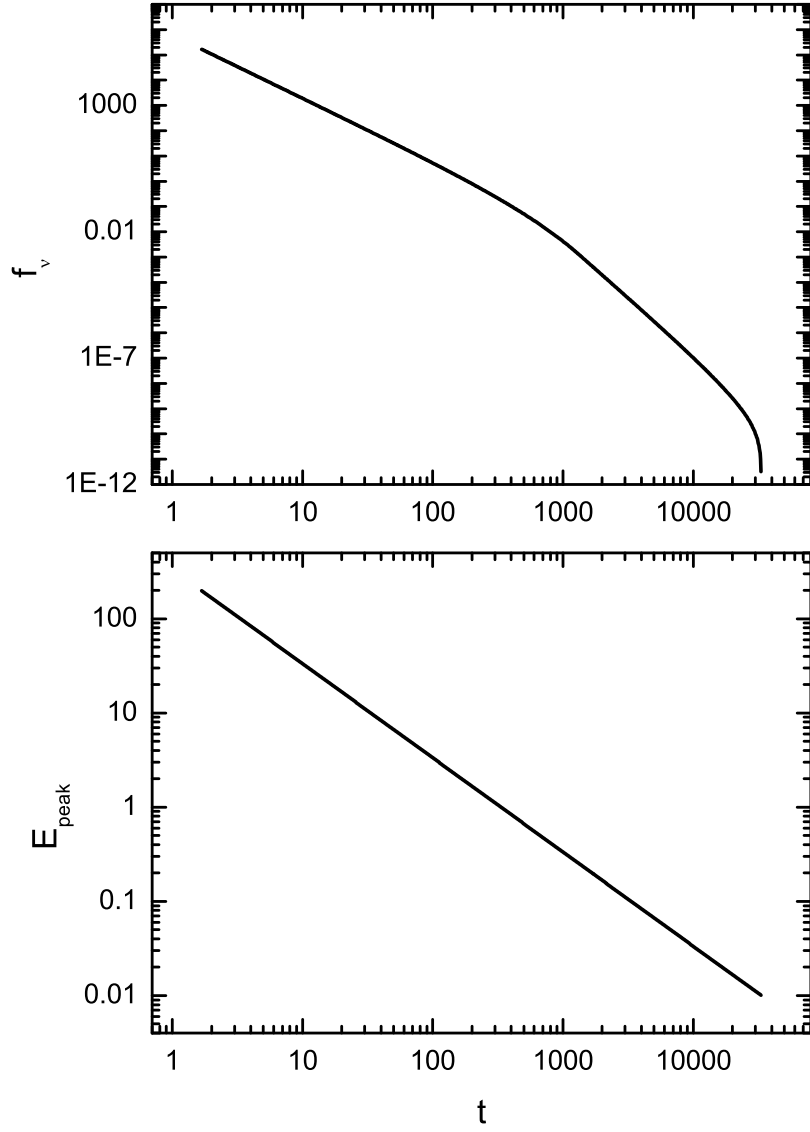


Fig. 3.— Evolution of the peak energy  $E_{peak}$  (the lower panel) of the observed spectrum of the emission considered in Fig. 1, where the light curve (the upper panel) is the same in Fig. 1.

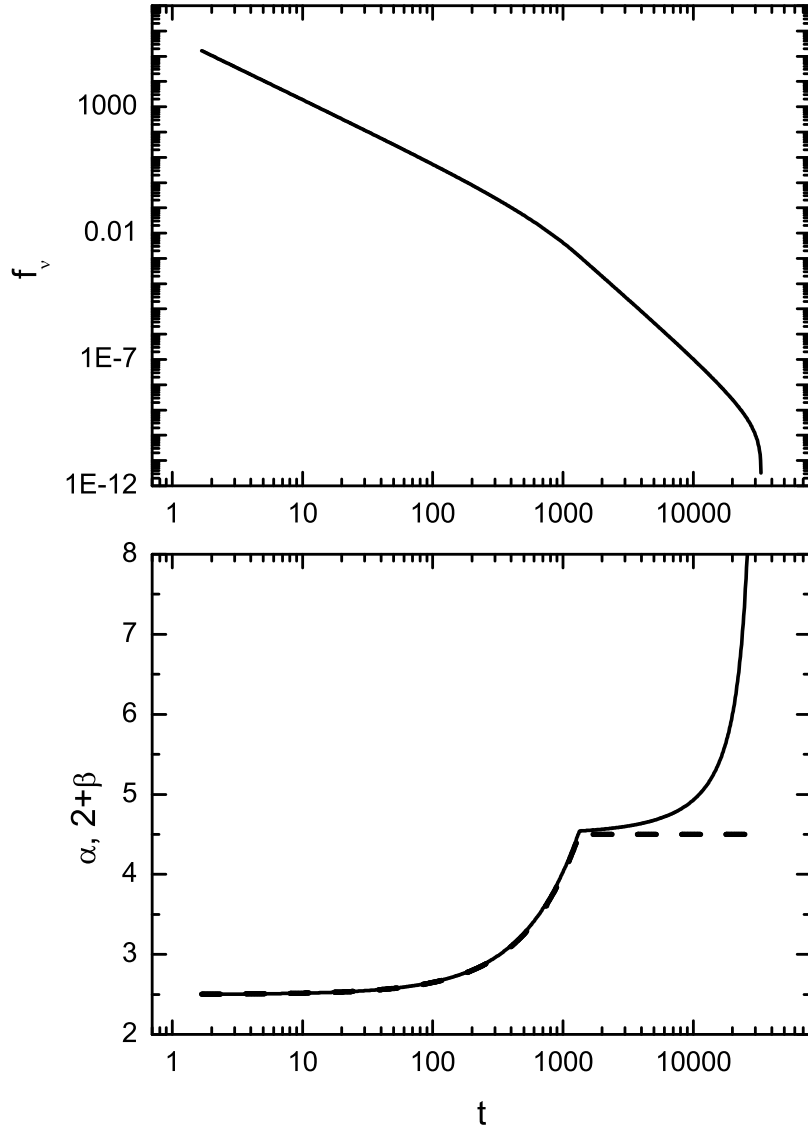


Fig. 4.— Comparison of the temporal index  $\alpha$  (the solid line in the lower panel) and spectral index  $\beta$  (presented in  $2 + \beta$ ) (the dash line in the lower panel) of the emission considered in Fig. 1, where the light curve (the upper panel) is the same in Fig. 1.

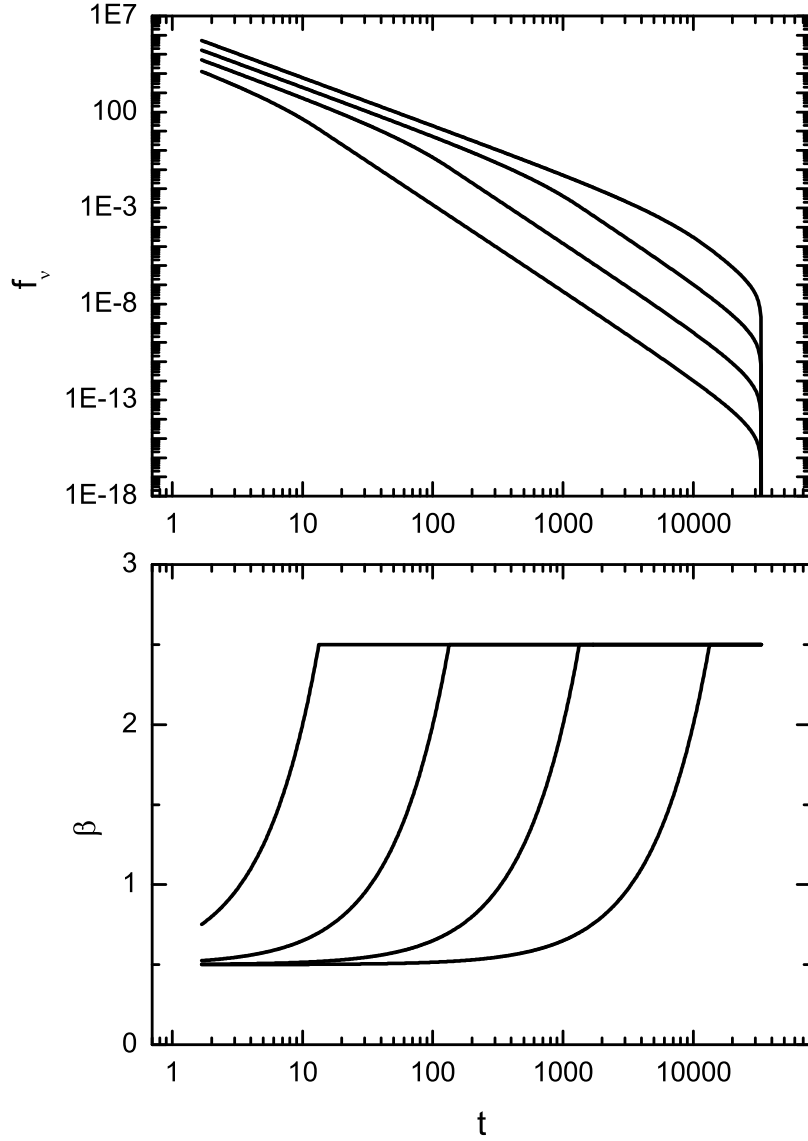


Fig. 5.— Comparison of the light curve (the upper panel; the units are the same as in Fig. 1) and the spectral evolution (the lower panel) of the same emission considered in Fig. 1, expected at different observation frequencies. In the lower panel, solid lines from the left to the right correspond to observation frequencies 100, 10, 1, and 0.1 keV respectively, whilst in the upper panel, solid lines from the bottom to the top are associated with 100, 10, 1, and 0.1 keV respectively.

## 5. Parameters that affect the results

The light curve and spectral evolution discussed in last section are produced by adopting a certain set of parameters. Here we investigate how these parameters affect the results.

### 5.1. Lorentz factor, fireball radius and peak energy of the intrinsic spectrum

The softening time scale exhibited in Fig. 1 must be affected by the Lorentz factor, fireball radius and peak energy of the intrinsic spectrum. We repeat the above analysis by replacing  $\Gamma = 100$ ,  $R_c = 10^{15}cm$  and  $h\nu_{0,p} = E_{0,p} = 1keV$  with  $\Gamma = 10$ ,  $R_c = 10^{14}cm$  and  $h\nu_{0,p} = E_{0,p} = 0.1keV$  one by one. The results are displayed in Fig. 6.

We find that a smaller Lorentz factor extend both the light curve (marked by its breaking feature which corresponds to the moment when the peak energy passes through the observation frequency) and the spectral softening to a larger time scale. This must be resulted from the less contraction of time. The cutoff tail of the steep decay phase remains in the same time position. This is not surprise since the tail is associated with the fireball radius, entirely independent of the Lorentz factor (see Qin 2008).

As expected, in the case of  $R_c = 10^{14}cm$ , the softening and the cutoff tail (as well as the breaking feature) shift to earlier time. The softening appears as early as  $< 3$  s and ends as early as  $\sim 100$  s, and the cutoff tail appears at  $\sim 3000$  s. At  $60s$  we find  $f_\nu \sim 0.3F_0$ , and at  $3000s$  (where the light curve cutoff tail appears)  $f_\nu \sim 1 \times 10^{-9}F_0$ . For this adopted parameter set, the flux at  $3000s$  is smaller than that at  $60s$  about 8 orders of magnitude, which is only 1 order of magnitude smaller than the usual observation magnitude range (7 orders). The undetectable problem raised above is now largely eased.

In the case of  $h\nu_{0,p} = E_{0,p} = 0.1keV$ , the spectral softening curve is almost overlapped with that of  $R_c = 10^{14}cm$ . Compared with the case of  $h\nu_{0,p} = E_{0,p} = 1keV$ , the breaking feature shifts to earlier time, whilst the cutoff tail remains in the same time position.

We notice from Fig. 6 together with Fig. 5 that the softening process, associated with various parameters, spans a time scale comparable to the terminating softening time  $t_{s,max}$ . In terms of mathematics, this is due to the fact that, relative to the moment  $t = 0$ , the start time of the softening is much smaller (more than one order of magnitude smaller) than  $t_{s,max}$ . We come to this conclusion: the time interval of the softening is in the same order of magnitude of the terminating softening time, and the two quantities much be linearly correlated. We suspect that it is the geometric property of the fireball surface that gives rise to this relation.

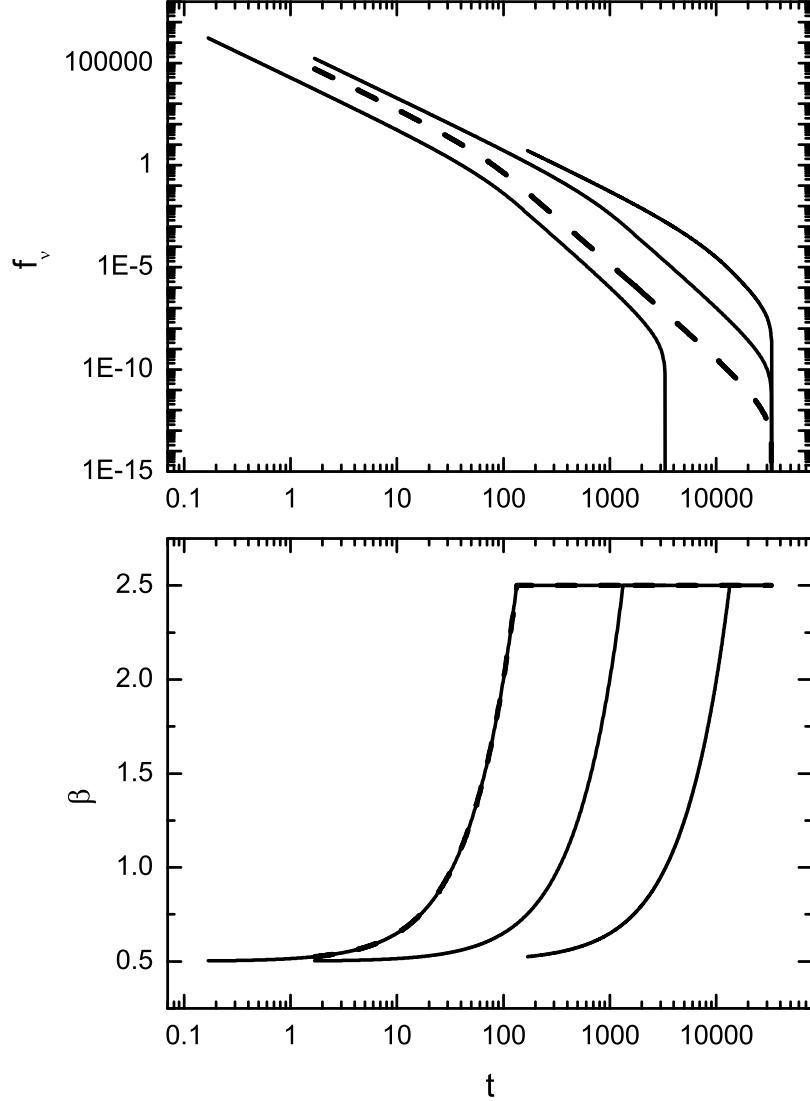


Fig. 6.— The light curve (the upper panel) and spectral evolution (the lower panel) of the emission considered in Fig. 1 (in the same units), produced by replacing the parameters adopted there. In the lower panel, solid lines from the left to the right correspond to the cases of replacing  $R_c = 10^{15}cm$  with  $R_c = 10^{14}cm$ , without replacement, and replacing  $\Gamma = 100$  with  $\Gamma = 10$ , respectively, and the dash line corresponds to the case of replacing  $h\nu_{0,p} = 1keV$  with  $h\nu_{0,p} = 0.1keV$ . In the upper panel, solid lines from the bottom to the top are associated with the cases of replacing  $R_c = 10^{15}cm$  with  $R_c = 10^{14}cm$ , without replacement, and replacing  $\Gamma = 100$  with  $\Gamma = 10$ , respectively, and the dash line corresponds to the case of replacing  $h\nu_{0,p} = 1keV$  with  $h\nu_{0,p} = 0.1keV$ .

## 5.2. High and low energy spectral indexes

High and low energy spectral indexes of the Band function must have influences on the spectral softening. We replace  $1 + \alpha_{B,0} = -0.5$  with  $1 + \alpha_{B,0} = 0$  and  $1 + \alpha_{B,0} = -0.8$ , and replace  $1 + \beta_{B,0} = -2.5$  with  $1 + \beta_{B,0} = -2$  and  $1 + \beta_{B,0} = -5$  respectively to produce the light curve and the spectral evolutionary curve. In doing so, other parameters remain unchanged.

The results are shown in Fig. 7. As expected, both indexes have influences on the softening curve: the low energy index  $\alpha_{B,0}$  puts a lower limit to the observed spectral index  $\beta$ , making  $\beta_{min} = -(1 + \alpha_{B,0})$ ; and the high energy index  $\beta_{B,0}$  confines the upper limit of  $\beta$ , following  $\beta_{max} = -(1 + \beta_{B,0})$ . The ratio between the fluxes at 60s and at 3000s is also influenced by the indexes, making the undetectable problem to be eased or worse.

Combining Figs. 5 and 7 we come to the following conclusions: the observed  $\beta_{min}$  and  $\beta_{max}$  are determined by the low and high energy indexes of the observed Band function spectrum (note that in the case of  $\delta$  function emission the observed spectrum and the intrinsic spectrum share the same form); the observed  $\beta_{min}$  and  $\beta_{max}$  for different observation frequencies would be unchanged as long as the whole softening process appears within the whole available observation time at the concerned frequencies.

## 6. Application

### 6.1. The light curve and spectral evolution expected in the XRT band

Our theoretical analysis carried above does not directly correspond to real observational data. In fact, instead of being defined at a particular observation frequency, the XRT light curve is measured within an energy band which is 0.3 – 10 keV. Therefore, it is necessary to investigate the light curve as well as the spectral evolution over this energy range. The available flux of the XRT light curve is always that has been integrated over this band. We use  $f_{\nu,int}$  to denote this flux which is determined by

$$f_{\nu,int}(t) = \int_{0.3keV}^{10keV} f_{\nu}(t) d\nu. \quad (14)$$

The flux is now in units of  $erg \cdot cm^{-2} s^{-1}$ .

There is a difficulty in evaluating the spectral index over a band. If the band is large enough one might not be able to consider it acting still as a power-law. Although we can impose a power-law on the spectrum over this band, the power-law index is still hard to be

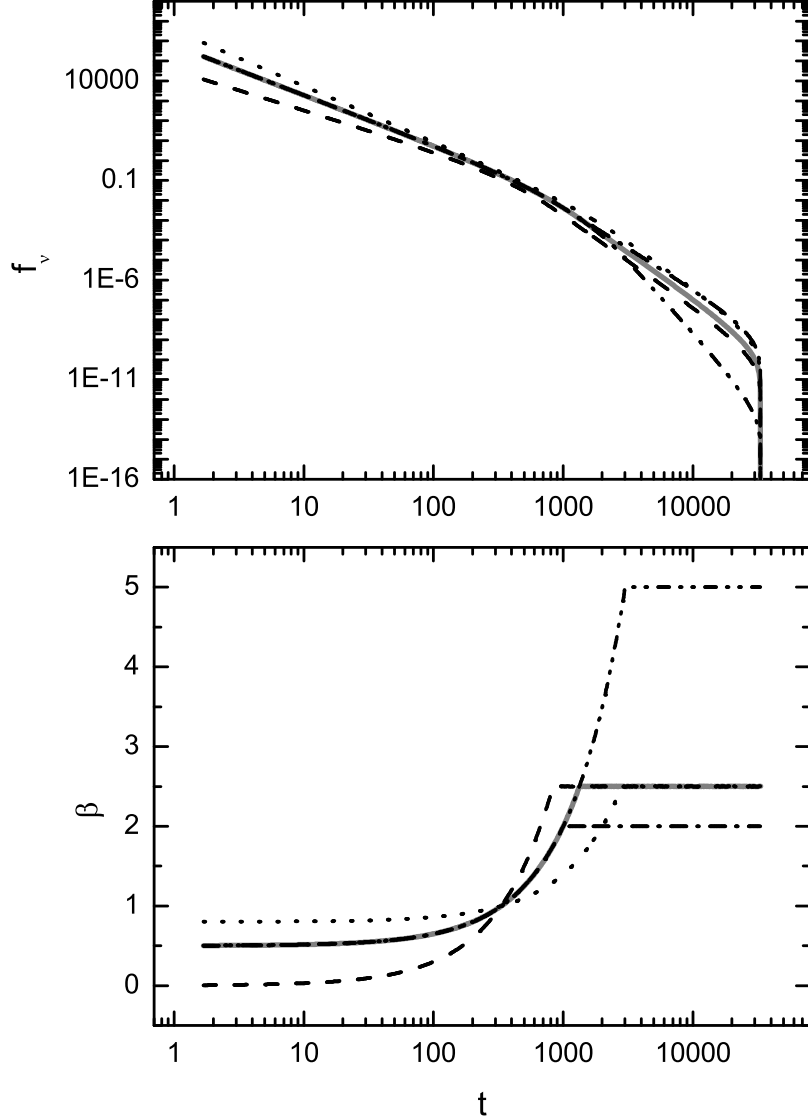


Fig. 7.— The light curve (the upper panel) and spectral evolution (the lower panel) of the emission considered in Fig. 1 (in the same units), produced by replacing the indexes adopted there. The dash, dot, dash dot, and dash dot dot lines correspond to the cases of replacing  $1 + \alpha_{B,0} = -0.5$  with  $1 + \alpha_{B,0} = 0$ , replacing  $1 + \alpha_{B,0} = -0.5$  with  $1 + \alpha_{B,0} = -0.8$ , replacing  $1 + \beta_{B,0} = -2.5$  with  $1 + \beta_{B,0} = -2$ , and replacing  $1 + \beta_{B,0} = -2.5$  with  $1 + \beta_{B,0} = -5$ , respectively. The two solid lines in Fig. 1 are presented in gray solid lines.

defined and hence hard to be determined. In terms of observation, we can collect all data points within this band and then figure out the index by performing a power-law fit. This method is hard to be adopted in theoretical investigation since one can create countless data points. We therefore turn to consider a simpler but well defined approach. First, we assume a power-law over the whole XRT band and then calculate the index by considering only the fluxes at the lower (0.3 keV) and upper (10 keV) limits of the band. Second, a power-law is assumed over a smaller band (0.6 – 5 keV) and then the index is calculated by employing only the fluxes at the new lower (0.6 keV) and upper (5 keV) limits. Presented in Fig. 8 are the spectral evolution so evaluated and the light curve of (14), where the Band function is also adopted and parameters other than the observation frequency are the same as those adopted in Fig. 1.

The upper panel of Fig. 8 shows that the XRT light curve is very similar to the 1 keV light curve. The power-law index  $\alpha$  of the former seems slightly different from that of the latter. This will lead to a deviation from the  $\alpha = 2 + \beta$  relation. From the lower panel we find that the lower and upper limits of the corresponding spectral index ( $\beta_{min}$  and  $\beta_{max}$ ) are the same as that measured at 1 keV, but the spectral evolutionary curve deviates significantly from that measured at 1 keV. The deviation is so large that the  $\alpha = 2 + \beta$  relation would be violently violated. This might help us to understand why this relation is not commonly detected. The lower panel also shows that the narrower the power-law range assumed, the closer the spectral evolutionary curve to that measured at 1 keV. This suggests that, the narrower band to concern, the more chance of detecting the  $\alpha = 2 + \beta$  relation.

## 6.2. GRB 060614

Although the condition that the emission is extremely short might be rare, there might be some bursts their early X-ray emission can roughly be accounted for by equation (11). Once a burst is selected, there are two ways of testing. One is to directly fit the light curve data and the spectral data with equation (11). The other is to check if their temporal and spectral indexes obey the  $\alpha = 2 + \beta$  relation. We adopt the second method since the result does not depend on fitting parameters.

Among the bursts (up to March 28, 2008) analyzed by the UNLV GRB Group (see <http://grb.physics.unlv.edu>), GRB 060614 might be one of such bursts that can be accounted for by the  $\delta$  function emission curvature effect model. There is an obvious softening in the steep decay phase for this burst. The light curve in this phase is relatively smooth, suggesting that, besides the main decay emission, it is unlikely that other components obviously influence the light curve. In this way, the temporal index can be well evaluated.

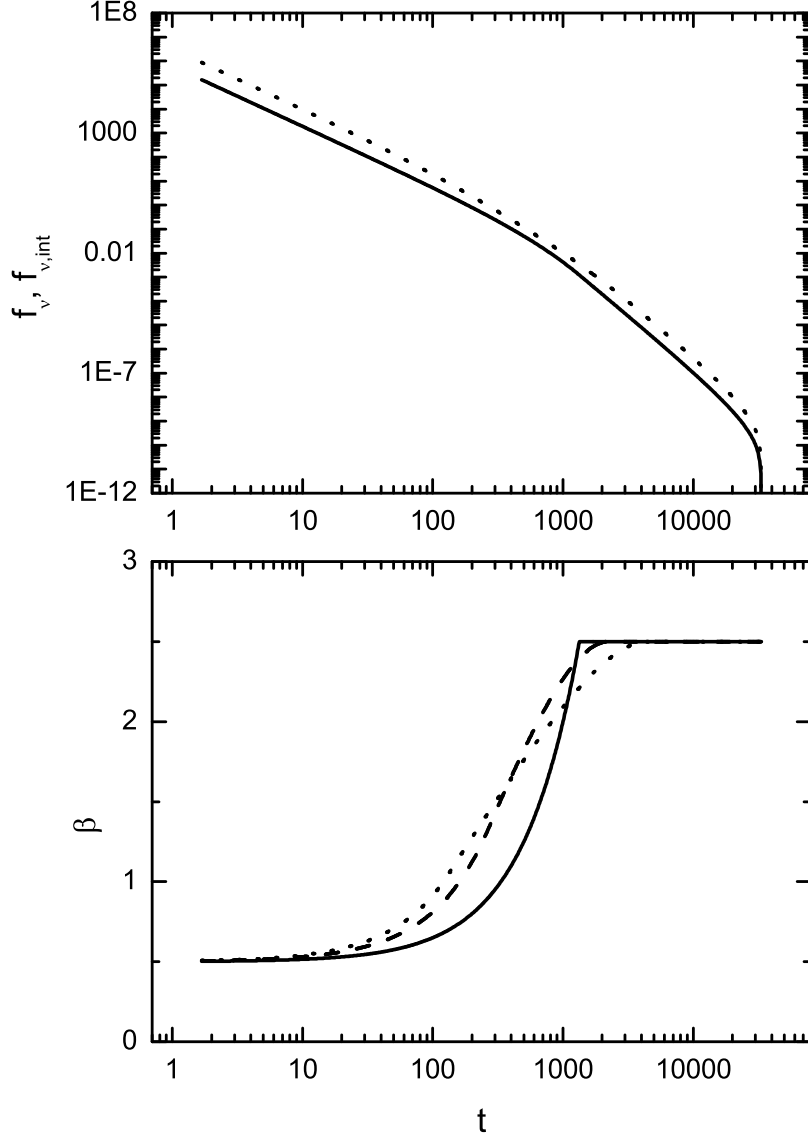


Fig. 8.— The light curve over the XRT band (the dot line in the upper panel; in unites of  $F_0 keV$ ) and the corresponding spectral evolution (the lower panel) of the emission considered in Fig. 1. The dot line in the lower panel represents the spectral index evaluated by considering a power-law spanning from 0.3 keV to 10 keV; the dash line stand for that calculated by assuming a power-law spanning from 0.6 keV to 5 keV. For the sake of comparison, both solid lines in Fig. 1 (in the same units as adopted there) are also presented.

According to the quality of the light curve data of this burst, we divide them into five sections in this phase, requiring that, for each section,  $\log f_\nu$  and  $\log t$  are linearly correlated. We then estimate the temporal index in each section by fitting the corresponding data with a power law function. Time intervals of these sections as well as the fitting results (the estimated temporal index  $\alpha$ ) are listed in Table 1, where  $t_1$  and  $t_2$  are the lower and upper limits of the observation time of the corresponding sections respectively.

The temporal index obtained from the light curve by the fit and the spectral index measured in the X-ray band by the UNLV GRB Group are presented in Fig. 9. We find that the  $\alpha - 2$  vs.  $t$  curve is roughly in agreement with the  $\beta$  vs.  $t$  curve in the concerned steep decay phase, suggesting that the curvature effect might probably be the main cause of the steep decay curve.

As analyzed in last subsection, the  $\alpha = 2 + \beta$  relation will not be strictly obeyed if one considers the light curve and the spectral index over a band (here, the XRT band) instead of at a fixed frequency. A deviation between the  $\alpha - 2$  vs.  $t$  curve and the  $\beta$  vs.  $t$  curve is hence expectable. However, the temporal index measured in the last time section in this phase is so large that it is likely to have other causes. Although the effect of the light curve over a band and the effect of the duration of the intrinsic emission have not been considered, we still suspect that the large temporal index might be a consequence of larger absorption for higher latitude photons.

## 7. Discussion and conclusions

We investigate the influence of the curvature effect on both the light curve and the spectrum of late emission of GRBs, attempting to explain the observed softening phenomenon in early X-ray afterglows of Swift. As the first step of investigation, we explore only the case

Table 1. Temporal indexes of GRB 060614.

section	$t_1$ (s)	$t_2$ (s)	$\alpha$
1	103.3	126.8	$2.73 \pm 0.23$
2	126.8	168.8	$2.25 \pm 0.13$
3	169.3	309.8	$3.841 \pm 0.064$
4	315.0	408.4	$3.78 \pm 0.25$
5	408.4	468.8	$5.89 \pm 0.48$

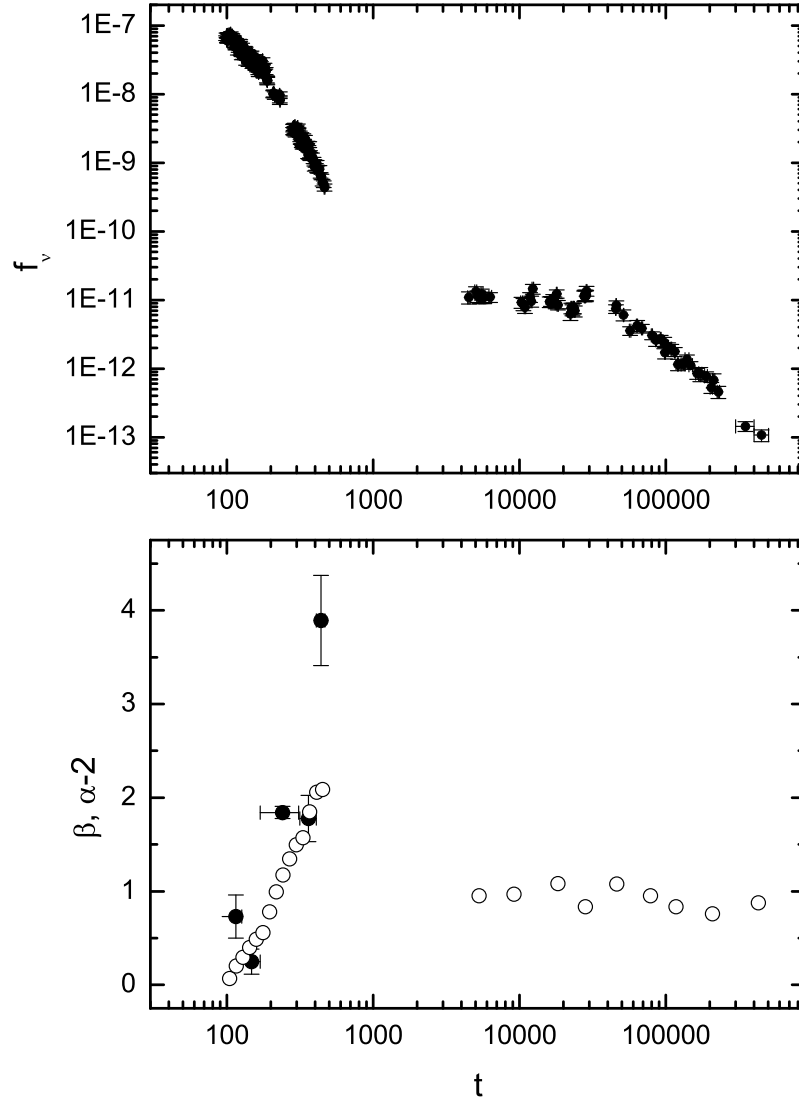


Fig. 9.— Comparison of the temporal index in  $\alpha - 2$  (the filled circles in the lower panel) and spectral index  $\beta$  (the open circles in the lower panel) of GRB 060614 in its steep decay phase. The data of the flux (the upper panel; in units of  $erg \cdot cm^{-2} s^{-1}$ ) and  $\beta$  are taken from the UNLV GRB Group website.

of extremely short intrinsic emission, for which we assume and apply a  $\delta$  function emission. Although how an emission is extremely short is currently unclear (this deserves a detailed investigation in the near future) and the condition that the emission is extremely short might be rare, the investigation is necessary since by considering such emission the possible impacts from the emission duration can be ignored and then the pure curvature effect can plainly be illustrated.

Formulas presented in Qin (2008) are employed to study this issue. Unlike what investigated in Qin (2008) and other relevant theoretical analyses (e.g., Fenimore et al. 1996; Sari et al. 1998; Kumar & Panaitescu 2000), we do not limit our study on an intrinsic power law spectrum. Instead, we consider more general spectral form of emission. Assuming a  $\delta$  function emission we get formulas that get rid of the impacts from the intrinsic emission duration, which are applicable to any forms of spectrum. According to these formulas, one would observe the same form of spectrum at different times, with the peak energy of the spectrum shifting from higher energy bands to lower bands. This was detected recently in the early X-ray afterglows of some GRBs (see Butler & Kocevski 2007). The peak energy is expected to decline following  $E_{peak} \propto t^{-1}$ . In the case when the emission is early enough so that the emitting area on the fireball surface is not far from the line of sight (say,  $\theta \ll \pi/2$  or  $t \ll R_c/v$ ), the temporal power law index and the spectral power law index will be well related by  $\alpha = 2 + \beta$ . As a consequence, the form  $t^2 f_\nu(t)$  will possess exactly the intrinsic spectral form (say, when replacing  $t$  with  $\nu$  one will get from  $t^2 f_\nu(t)$  as a function of  $\nu$  that take exactly the same form of the intrinsic spectrum). The  $\alpha = 2 + \beta$  relation will be broken down and  $\alpha > 2 + \beta$  or  $\alpha \gg 2 + \beta$  will hold (see Fig. 4) at much later time when the angle between the moving direction of the emission area and the line of sight is large.

As revealed in Butler & Kocevski (2007) and suggested by Starling et al. (2008), we focus our attention to the emission with a Band function spectrum. This spectrum has a power law behavior in both lower and higher energy bands, where the two power laws are smoothly connected (Band et al. 1993). Using this spectral form, we plot the light curve and the spectral evolution with our formulas, expected at 1 keV and other frequencies. The analysis shows that there do exist a temporal steep decay phase and a spectral softening which occur simultaneously. As Fig.2 reveals, both the steep decay light curve and the spectral softening are caused by the shifting of the Band spectrum. As mentioned above, Starling et al. (2008) suggested that the steep decline in the flux of GRB 070616 may be caused by a combination of the strong spectral evolution and the curvature effect. Based on the above argument, we insist that both the spectral evolution and the steep decline observed in GRB 070616 and other Swift bursts are likely to be caused merely by the curvature effect. In addition, we find that, just as what is illustrated in Qin (2008), the  $\cos\theta$  term,  $R_c/v - t$ , plays a role in producing the light curve, which “attaches” a cutoff tail to the latter (see

Fig. 1). The spectral softening terminates when the emission is dominated by that from the high energy portion of the Band function spectrum. Thus, there exists a maximum of the spectral index,  $\beta_{max}$ . After the  $\beta_{max}$  appears, it lasts to the end of the emission, including the phase of the cutoff tail. Our analysis shows that the softening due to the curvature effect will appear at different frequencies; it occurs earlier for higher frequencies and later for lower frequencies; a characteristic of the softening, the terminating softening time  $t_{s,max}$  (when the  $\beta_{max}$  appears), depends strictly on the observation frequency, which follows  $t_{s,max} \propto \nu^{-1}$ . Although this is concluded based on the assumption of extremely short emission, we tend to believe that its main characters hold in most cases since the light curve from any finite emission is contributed by countless  $\delta$  function emission. The combination of these countless  $\delta$  function emission would change the values of some quantities such as  $t_{s,max}$ , but would not change the trend. Starling et al. (2008) showed, the spectral evolution of GRB 070616 starts earlier at  $\gamma$ -ray energies (while the X-ray flux is still at an approximately constant level) and begins much later at X-ray energies around the onset of the steep X-ray decay. In terms of the curvature effect, this is due to the following fact: the peak energy of the Band function spectrum passes through the  $\gamma$ -ray band at a relatively early time, while it passes through the X-ray band at a later time.

Parameters that might have impacts on the light curve and the spectral evolution are also studied. Whilst a smaller Lorentz factor shifts the spectral softening to larger time scales, smaller values of the fireball radius and the rest frame peak energy make the occurrence of the softening earlier. The analysis shows that the terminating softening time appears much later than the start time of the softening. The former is always larger than the latter by about one order of magnitude. It is therefore predicted that the duration of the softening and the terminating softening time would be linearly correlated. It also shows that the low energy index  $\alpha_{B,0}$  puts a lower limit to the observed spectral index  $\beta$  and the high energy index  $\beta_{B,0}$  confines the upper limit of  $\beta$ . The following conclusions are reached: the observed  $\beta_{min}$  and  $\beta_{max}$  are determined by the low and high energy indexes of the observed Band function spectrum;  $\beta_{min}$  and  $\beta_{max}$  for different observation frequencies would remain unchanged as long as the whole softening process appears within the whole available observation time at the concerned frequencies.

As application, we study the light curve and the spectral evolution over the XRT band. That is, the light curve is that has been integrated over the 0.3–10 keV band and the spectral index is estimated by assuming a power-law over this band. The analysis shows that the light curve slightly deviate from that measured at 1 keV, whilst the spectral evolutionary curve significantly betrays that measured at 1 keV. This suggests that the  $\alpha = 2 + \beta$  relation will be violently violated if one measures the light curve and estimates the spectral index over a wide band.

Another application is to check the  $\alpha = 2 + \beta$  relation by employing the light curve and spectrum data of GRB 060614. The temporal index  $\alpha$  in the steep decay phase of this burst is evaluated. We compare  $\alpha$  and the spectral index  $\beta$  in the same softening phase (it is also the steep decay phase of the light curve). It shows that the  $\alpha - 2$  vs.  $t$  curve and the  $\beta$  vs.  $t$  curve are roughly in agreement, suggesting that the  $\alpha = 2 + \beta$  relation is roughly satisfied in this phase and the softening of this burst might possibly be due to the curvature effect.

What we have investigated are based on the assumption of extremely short emission which ignores the possible impacts from the emission duration. While the contribution of the emission duration might have less affect on the spectrum, it might obviously affect the temporal profile and hence the temporal index. Therefore the  $\alpha = 2 + \beta$  relation might not hold in this case. Combining this with the problem arising from the estimation of the spectral index in the softening phase over an energy band rather than at a fixed frequency, it might be able to explain why the  $\alpha = 2 + \beta$  relation is not common in Swift bursts (see Liang et al. 2006 and also Zhang 2007 for a detailed discussion). Yonetoku et al. (2008) showed that the two characteristic break energies they considered have a time dependence of  $\propto t^{-3} - t^{-4}$ . This is not in agreement with the prediction of the  $E_{peak} \propto t^{-1}$  law. Perhaps an intrinsic softening might be responsible for this difference when the emission duration is taken into account. Another possibility is that the  $E_{peak}$  shifting of this kind of burst is due to structure jets, where in high latitude,  $E_{peak}$  would be much smaller than it is in uniform jets. In addition to test the  $\alpha = 2 + \beta$  relation and the  $E_{peak} \propto t^{-1}$  law, we suggest to detect the softening at different frequencies as well. The observed relations might not strictly follow what the  $\delta$  function emission model predicts, but as argued above, the trend of the relevant effects would be maintained (which deserves a detailed investigation in the near future).

In addition to these more conventional tests, we propose to try a totally new test which is to check if the  $t^3 f_\nu(t)$  vs.  $t$  curve is in agreement with the  $\nu f_\nu$  vs.  $\nu$  curve when replacing  $t$  with  $\nu$  in the  $t^3 f_\nu(t)$  and  $t$  forms and multiplying a constant to match the corresponding dimensions (see Section 3). Illustrated in Fig. 10 is an example of the comparison (where we compare only the relevant functions and thus do not replace variables or multiply constants to change the dimensions). An advantage of doing so is that we can guess spectrum form merely from the light curve data. For example, when we find that the  $t^3 f_\nu(t)$  form being a perfect power-law function of time, then the spectrum is guessed to be a pure power-law (if the spectral data are found not to obey a power-law, then we will have reasons to doubt if this burst is not affected by the curvature effect). Or, when we find that the  $t^3 f_\nu(t)$  form is a Band function of time, then we will have reasons to guess that the spectrum takes a Band function form. Another usage of plotting the  $t^3 f_\nu(t)$  vs.  $t$  curve is to find out the time when the peak energy passes through the observation band (see also Kumar & Panaitescu 2000), which can be directly checked by observation and hence becomes a test to the curvature

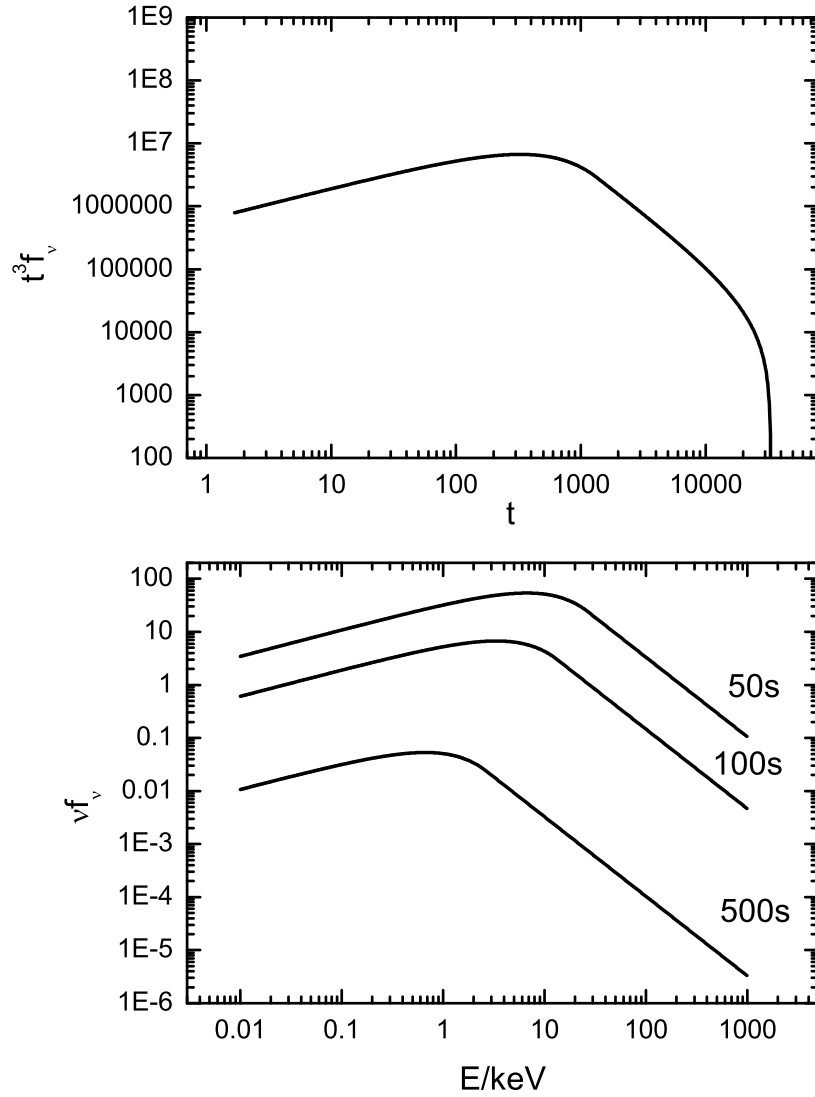


Fig. 10.— Comparison of the functions of the  $t^3 f_\nu(t)$  vs.  $t$  curve (the upper panel) and the  $\nu f_\nu$  vs.  $\nu$  curve (the spectrum; the lower panel) of the emission considered in Fig. 1. The three solid lines in the lower panel are the same lines of 50, 100, and 500 s respectively in Fig. 1.

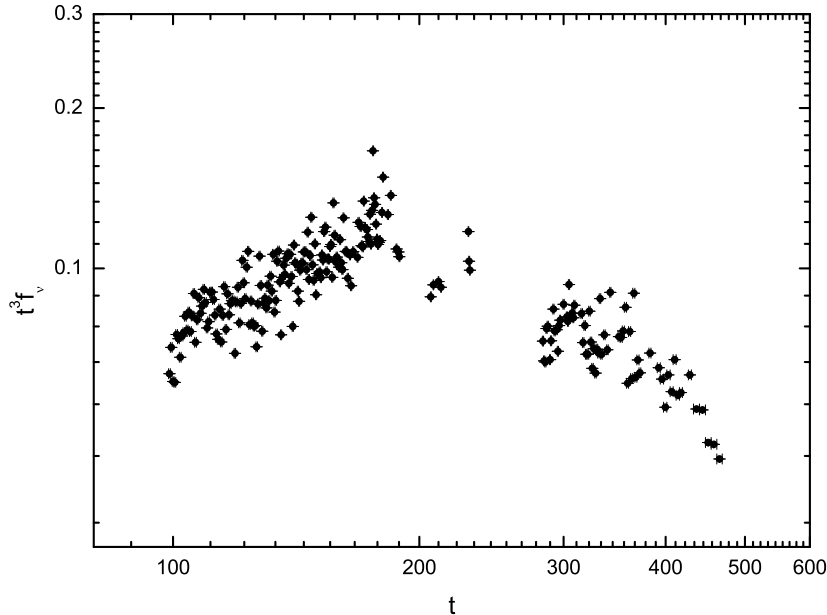


Fig. 11.— The  $t^3 f_\nu(t)$  (in units of  $erg \cdot cm^{-2} s^2$ ) vs.  $t$  curve of GRB 060614 in its steep decay phase. The data are taken from the UNLV GRB Group website.

effect as well. According to equation (11), the moment when the peak of  $t^3 f_\nu(t)$  appears is the time when the peak energy passes through the observation frequency  $\nu$ , or, it is the time when  $E_{peak} = h\nu$ . In plotting the  $t^3 f_\nu(t)$  vs.  $t$  curve (see the upper panel of Fig. 10), one can also check the influence of factors other than that of the pure curvature effect by observing and measuring the deviation of a real light curve from that of equation (11). An extra usage of this plot might be a direct comparison of light curves of different bursts, probably enabling us to divide them according to their temporal properties (we strongly suggest a detailed investigation on this issue in the near future).

Displayed in Fig. 11 is the  $t^3 f_\nu(t)$  vs.  $t$  curve of GRB 060614. It shows a function of time bearing the Band function form (when replacing  $\nu$  with  $t$ ) attached with a cutoff tail. If we believe that the softening of this burst is due to the curvature effect in the case of extremely short emission, according to Fig. 11 it would be expectable that the peak energy of this burst passes through the corresponding observation energy range (the XRT band) at  $\sim 175$  s (or, at  $\sim 175$  s, the peak energy of the observed spectrum is just within the energy

range of the light curve). Indeed, as presented in Table 4 of Mangano et al. (2007), within the time interval 128–190 s, the peak energy (when fitting the spectrum with a Band model) is about 2–4 keV which is well within the 0.3–10 keV band. A similar result for this burst is also visible in Fig. 1 of Butler & Kocevski (2007).

Based on their fits to the composite light curves, Sakamoto et al. (2007) confirmed the existence of an exponential decay component which smoothly connects the BAT prompt data to the XRT steep decay for several GRBs. Yonetoku et al. (2008) also showed that the spectrum of GRB 060904A contains a cutoff tail in its higher energy range, which can be represented by an exponential function. According to the above analysis, the spectral form obviously affects the light curve if the curvature effect is at work and the intrinsic emission is short enough. An intrinsic spectrum with an exponential tail might probably lead to an exponential decay light curve. We notice that the projected factor (the  $\cos\theta$  term) also produces a very steep decay phase when the angle between the moving direction of the dominant emission area and the line of sight is large enough. However, it is unlikely that many of them (if not only few of them) are due to the  $\cos\theta$  term, since this term always appears at a very late time (see Fig. 6 and also Qin 2008). The following factors might also be the cause of this tail: one is the large absorption for higher latitude emission and the other is the limited open angle of jets. Both will lead to a steeper tail. While the former might probably give rise to a smooth decay curve, the latter might probably lead to a sharp feature.

In addition to the shifting of the peak energy, Starling et al. (2008) also observed softening of the low energy power law slope. They measured a softening of the low energy spectral slope from  $\alpha \sim 0.1 - 1.3$ . This implies that the intrinsic spectrum might evolved itself. This cannot be taken into account in the current investigation since a  $\delta$  function emission has no evolution. We suggest to explore in a later investigation the impact from the emission duration and the effect from the intrinsic spectral evolution.

Special thanks are given to the anonymous referee for his or her comments and suggestions which have improved the paper greatly. This work was supported by the National Natural Science Foundation of China (No. 10573005 and No. 10747001) and by the Guangzhou Education Bureau and Guangzhou Science and Technology Bureau.

### A. Projected factor as a function of time

Emission from a distant area is proportional to the projected factor of the area relative to the observer, which is known as  $\cos\theta$ , where  $\theta$  is the angle between the normal of the

area and the line of sight. For a face-on area (its normal is parallel to the line sight),  $\theta = 0$  and then  $\cos\theta = 1$ ; and for an edge-on area (its normal is perpendicular to the line sight),  $\theta = \pi/2$  and then  $\cos\theta = 0$ . The projected factor varies from  $\cos\theta = 1$  to  $\cos\theta = 0$  for the half fireball surface facing the observer. Due to time delation, emission from the area of  $\theta = 0$  reaches the observer earlier and that of  $\theta = \pi/2$  reaches the observer later, and the former emission is not reduced by the projected factor whilst the latter will be reduced to zero. It has been pointed out that the term  $R_c/v - t$  in equation (11) comes from nothing but the projected factor  $\cos\theta$  (Qin 2008). Here we analyze this issue in detail.

Taking into account the increase of the radius of an expanding fireball (equation A.3 in Qin 2002) and the time delay associated with different latitudes in the fireball surface (equation A.6 in Qin 2002), one obtains the following relation between the observation time  $t_{ob}$  and the angle relative to the line of sight (equation A.7 in Qin 2002)

$$t_{emit} = \frac{t_{ob} - D/c + [R_c/c - (v/c)t_c]\cos\theta}{1 - (v/c)\cos\theta}, \quad (\text{A1})$$

which could be written as

$$\cos\theta = \frac{t_{emit} + D/c - t_{ob}}{R_c/c + (v/c)(t_{emit} - t_c)}. \quad (\text{A2})$$

Replacing  $t_{ob}$  with  $t$  (see equation 1) and considering the time contraction  $t_{emit} - t_c = \Gamma(t_0 - t_{0,c})$  (equation A.1 in Qin 2002), we get

$$\cos\theta = \frac{(t_0 - t_{0,c})\Gamma + R_c/v - t}{[(t_0 - t_{0,c})v\Gamma + R_c]/c}. \quad (\text{A3})$$

As revealed in equation (A.4) in Qin (2002),  $(t_0 - t_{0,c})v\Gamma + R_c$  is the fireball radius measured at  $t_0$ . Equation (A3) suggests that, for any particular intrinsic emission time  $t_0$  (at which the fireball radius is fixed),  $\cos\theta$  varies with observation time  $t$ . This is due to the time delay, as mentioned above (see also equation A.6 in Qin 2002). According to equation (A3), the term  $(t_0 - t_{0,c})\Gamma + R_c/v - t$  in equation (2) is the projected factor  $\cos\theta$  multiplying the fireball radius divided by the speed of light. Note that the term  $(t_0 - t_{0,c})\Gamma + R_c/v - t$  in equation (2) directly comes from the term  $\cos\theta$  in equation (A.15) in Qin (2002) as a consequence of the projected effect (see equation A.11 in Qin 2002).

For the  $\delta$  function emission considered in this paper, the intrinsic emission is assigned to occur at  $t_0 = t_{0,c}$  (see equation 7), which leads to

$$\cos\theta = \frac{R_c/v - t}{R_c/c}. \quad (\text{A4})$$

This explains why we interpret the term  $R_c/v - t$  in equation (11) as that reflecting the projected factor of the emission area in the fireball surface.

Note that observation time  $t$  is confined by equation (8) which arises from the limit of the fireball surface in the case of  $\delta$  function emission (see Qin 2002; Qin et al. 2004; Qin 2008). According to equation (A4),  $\cos\theta = 1$  when  $t = (1 - v/c)R_c/v$  which is the observation time when photons from the face-on area ( $\theta = 0$ ) of the fireball surface arrive the observer. When taking  $t = R_c/v$  we get  $\cos\theta = 0$ . Note that  $t = R_c/v$  is the observation time when photons from the edge-on area ( $\theta = \pi/2$ ) reach the observer.

In the case of  $R_c = 10^{15}cm$  and  $\Gamma = 100$ ,  $R_c/v \sim 3 \times 10^4s$  which is much larger than the steep decay segment of most GRBs detected by Swift. Even for  $R_c = 10^{14}cm$  we get  $R_c/v \sim 3 \times 10^3s$  which is still larger than the steep decay segment of many Swift GRBs. For the observation time satisfying  $t \ll R_c/v$ , the projected factor approaches a unit and then can be ignored. Only when the observation time is comparative to  $R_c/v$ , the projected factor will play an important role (see the broken down feature in Fig. 1). The broken down feature also exists in the case of the pure power-law spectrum (Qin 2008). When this feature is observed, the fireball radius will be well determined, no matter the observed spectrum is a pure power-law or a Band function form.

## B. Projected factor in flux

Here we show how the projected factor plays a role in the flux per unit frequency from a relativistic source.

As shown in Qin (2002), the amount of energy emitted from differential area  $ds_{emit}$  radiating towards the observer is

$$dE_{emit} = \frac{I_\nu \cos\theta ds_{emit} d\nu dt \Delta s_{ob}}{D^2}, \quad (B1)$$

where  $I_\nu$  is the intensity of radiation measured by local observers near the emitting source,  $\cos\theta$  is the projected factor of  $ds_{emit}$  towards the distant observer,  $d\nu$  and  $dt$  are the observed frequency and time intervals respectively,  $\Delta s_{ob}$  is the area of the detector, and  $D$  is the distance between the observer and the emitter. The flux density measured from this amount of energy is

$$df_\nu = \frac{I_\nu \cos\theta ds_{emit}}{D^2}. \quad (B2)$$

Observer frame intensity  $I_\nu$  is related with the intrinsic intensity  $I_{0,\nu}$  by

$$I_\nu = \left(\frac{\nu}{\nu_0}\right)^3 I_{0,\nu}, \quad (B3)$$

where  $\nu_0$  is the intrinsic frequency. Applying this relation and the Doppler effect we get

$$df_\nu = \frac{I_{0,\nu} \cos\theta ds_{emit}}{D^2 \Gamma^3 [1 - (v/c) \cos\theta]^3}. \quad (\text{B4})$$

If the area is on the tip of the fireball surface,  $\theta = 0$ . That gives rise to

$$df_{\nu,0} = \frac{I_{0,\nu} ds_{emit}}{D^2 \Gamma^3 [1 - (v/c)]^3}. \quad (\text{B5})$$

The relation between  $df_\nu$  and  $df_{\nu,0}$  is

$$\frac{df_\nu}{df_{\nu,0}} = \left[ \frac{1 - (v/c)}{1 - (v/c) \cos\theta} \right]^3 \cos\theta. \quad (\text{B6})$$

For a large Lorentz factor, we get

$$\frac{df_\nu}{df_{\nu,0}} = \frac{\cos\theta}{8\Gamma^6 [1 - (1 - 1/2\Gamma^2) \cos\theta]^3}. \quad (\text{B7})$$

Here are several particular results: a) when  $\theta \ll 1/\Gamma$ ,  $df_\nu/df_{\nu,0} = 1$ ; b) when  $1/\Gamma \ll \theta \ll 1$ ,  $df_\nu/df_{\nu,0} = 1/(\theta\Gamma)^6$ , which was previously pointed out by Kumar & Panaitescu (2000); c) when  $\theta = \pi/3$ ,  $df_\nu/df_{\nu,0} = 1/2\Gamma^6$ ; d) when  $\theta = \pi/2$ ,  $df_\nu/df_{\nu,0} = 0$ .

## REFERENCES

- Band, D. et al. 1993, ApJ, 413, 281
- Barthelmy, S. D. et al. 2005, ApJ, 635, L133
- Butler, N. R. & Kocevski, D. 2007, ApJ, 663, 407
- Campana, S. et al. 2006, Nature, 442, 1008
- Dado, S., Dar, A., Rujula, A. D. 2008, astro-ph/0709.4307
- Dermer, C. D. 2004, ApJ, 614, 284
- Dyks, J. et al. 2005, preprint, astro-ph/0511699
- Fan, Y. Z. et al. 2006, JCAP, 9, 13
- Fenimore, E. E. et al. 1996, ApJ, 473, 998

- Ghisellini, G. et al. 2006, MNRAS, 372, 1699
- Gehrels, N. et al. 2004, ApJ, 611, 1005
- Gehrels, N. et al. 2006, Nature, 444, 1044
- Jia, L.-W. 2008, ChJAA, 8, 451
- Kocevski, D., Ryde, F., Liang, E. 2003, ApJ, 596, 389
- Kumar, P., & Panaitescu, A. 2000, ApJ, 541, L51
- Liang, E. W. et al. 2006, ApJ, 646, 351
- Lu, R.-J., Qin, Y.-P., Zhang, Z.-B., Yi, T.-F. 2006, MNRAS, 367, 275
- Lu, R.-J., Peng, Z.-Y., Dong, W. 2007, ApJ, 663, 1110
- Mangano, V. et al. 2007, A&A, 470, 105
- Panaitescu, A. et al. 2006, MNRAS, 366, 1357
- Peng, Z.-Y., Qin, Y.-P., Zhang, B.-B., Lu, R.-J., Jia, L.-W., Zhang, Z.-B. 2006, MNRAS, 368, 1351
- Qin, Y.-P. 2002, A&A, 396, 705
- Qin, Y.-P. et al. 2004, ApJ, 617, 439
- Qin, Y.-P. & Lu, R.-J. 2005, MNRAS, 362, 1085
- Qin, Y.-P. et al. 2005, ApJ, 632, 1008
- Qin, Y.-P. et al. 2006, Phys. Rev. D 74, 063005
- Qin, Y.-P. 2008, ApJ, 683, 900
- Ryde, F., & Petrosian, V. 2002, ApJ, 578, 290
- Sakamoto, T. et al. et al. 2007, ApJ, 669, 1115
- Sari, R., & Piran, T. 1997, ApJ, 485, 270
- Sari, R., Piran, T., & Narayan, R. 1998, ApJ, 497, L17
- Shen, R.-F. et al. 2005, MNRAS, 362, 59

Starling, R. L. C. et al. 2008, MNRAS, 384, 504

Tagliaferri, G. et al. 2005, Nature, 436, 985

Yonetoku, D. et al. 2008, PASJ, 60, S351

Zhang, B. 2007, ChJAA, 7, 1

Zhang, B. et al. 2007a, ApJ, 655, L25

Zhang, B.-B. et al. 2007b, ApJ, 666, 1002

Zhang, B., Fan, Y. Z., Dyks, J. et al. 2006, ApJ, 642, 354